



HAL
open science

A Ku-Band Laboratory Experiment on the Electromagnetic Bias

Hubert Branger, Alfred Ramamonjiarisoa, Larry F. Bliven

► **To cite this version:**

Hubert Branger, Alfred Ramamonjiarisoa, Larry F. Bliven. A Ku-Band Laboratory Experiment on the Electromagnetic Bias. *IEEE Transactions on Geoscience and Remote Sensing*, 1993, 31 (6), pp.1165-1179. 10.1109/36.317446 . hal-00192501

HAL Id: hal-00192501

<https://hal.science/hal-00192501>

Submitted on 20 May 2023

HAL is a multi-disciplinary open access archive for the deposit and dissemination of scientific research documents, whether they are published or not. The documents may come from teaching and research institutions in France or abroad, or from public or private research centers.

L'archive ouverte pluridisciplinaire **HAL**, est destinée au dépôt et à la diffusion de documents scientifiques de niveau recherche, publiés ou non, émanant des établissements d'enseignement et de recherche français ou étrangers, des laboratoires publics ou privés.



Distributed under a Creative Commons Attribution 4.0 International License

A *Ku*-Band Laboratory Experiment on the Electromagnetic Bias

Hubert Branger, Alfred Ramamonjiarisoa, and Larry F. Bliven

Abstract—Sea-surface electromagnetic bias (EM bias), the difference between the mean reflecting surface and the geometric mean sea level, must be accurately determined to realize the full potential of satellite altimeters. A uniformly valid algorithm relating the normalized (or nondimensional) EM bias, i.e., “bias/significant wave height,” to physical variables has not yet been established, so we conducted laboratory experiments to guide model development. Simultaneous and collocated measurements of surface topography and altimeter backscattered power were made in the large IMST wind-wave facility for a wide range of wind and mechanically generated wave conditions. A small microwave footprint on the water surface was produced by a focused-beam 13.5 GHz radar system that has a high signal-to-noise ratio. Consequently specular facets are easily identifiable and the data show that troughs are on average better reflectors than crests.

Dimensional relations seldom yield robust algorithms and in fact, although rather high correlation is found between normalized EM bias and either wind speed or wave height, the laboratory coefficients are considerably greater than those of *in situ* algorithms. Nondimensional parameterization is more useful for deriving scaling laws, and when the normalized EM bias is displayed as a function of wave height skewness or wave age, laboratory and field data converge into consistent trends. In particular, normalized bias decreases with wave age, but unfortunately, even the wave age model does not account for the effects of mechanically generated waves, which produce appreciable scatter relative to the pure wind cases. Thus, we propose a two-parameter model using 1) a nondimensional wave height, which is computed for local winds, and 2) a significant slope, which is computed for nonlocally generated waves. Analysis of the laboratory data shows that the normalized EM bias for mixed conditions is well modeled as a product of these two parameters.

I. INTRODUCTION

SPACEBORNE radar altimeters are used to map mean sea level (msl), which is of crucial interest in geodetic, topographic, and large-scale ocean circulation studies. A radar altimeter is an active microwave instrument from which short pulses are transmitted vertically towards the sea-surface. When a pulse hits the ocean, the echo is partially reflected by specular facets towards a receiver on-

board the spacecraft. The round-trip travel time of the pulse is related to the altitude of the satellite above the sea. If the satellite orbit is known, then the altimeter range measurements can be used to determine the sea surface topography. Horizontal gradients of dynamic sea-surface topography provide a measure of oceanic geostrophic currents. The dynamic topography of a western boundary current like the Gulf Stream can be about 2 m, but many other gradients are so weak that a precision of few centimeters is required for msl measurements to be useful.

In fact, altimeter range measurements yield the mean reflecting surface level, which generally differs from the true msl—the deviation is known as *electromagnetic bias* (*EM bias*). The bias occurs because sea-surface roughness is spatially inhomogeneous. For microwave frequencies, troughs typically are better reflectors than crests so the level of the mean reflecting surface is usually lower than the true msl. EM bias can be large enough that it needs to be accounted for to get optimum use of altimeter data.

In spite of intense work since the first observation by Yapple *et al.* [1], there is still no robust EM bias empirical algorithm or analytical model. EM bias is a function of the joint wave height and wave slope probability density function (pdf), which is not measured. There is as yet no unique inversion algorithm for deriving EM bias from return waveforms [2], [3]. EM bias is primarily dependent upon sea-surface topography, but radar pointing angle [4]–[6] and radar frequency [7], [8] are also important. Skewness of the wave height distribution has been theoretically related to EM bias [9], and for suitable model assumptions, it can be deduced from the return waveform. But skewness estimates from waveforms are frequently not accurate enough for this method to provide an operational algorithm [10] so its operational use is questionable. As a result of these factors, potential operational algorithms are semi-empirical relationships that use 1) the significant wave height SWH, which is related to the rise time of the return waveform leading edge, and 2) the wind speed U , which is related to the backscattered radar cross section σ_o [11].

Considerable effort has been devoted to modeling EM bias, and comprehensive reviews of theoretical and experimental studies can be found in [3] and [12]. Table I summarizes assorted theoretical and observational expressions for computing the so-called *normalized or nondimensional EM bias*, $\beta = EM\ bias/SWH$. Relationship based on the cross-skewness coefficient γ (formula (3) in

Manuscript received April 24, 1992; revised March 11, 1993. This work was supported in part by CNES Contract E/57 90/8002/854, Conseil Regional PACA Contract 90/04594/00, ONR Contract 972/146/70/11, and NASA Contract RTOP 972/161/80/28.

H. Branger and A. Ramamonjiarisoa are with the Institut de Mécanique Statistique de la Turbulence, 12, Leclerc av. Marseille 13003, France.

L. F. Bliven is with the NASA Goddard Space Flight Center, Laboratory for Hydrospheric Processes, Wallops Flight Facility, Wallops Island, VA 23337.

TABLE I
THEORETICAL AND OBSERVATIONAL (Ku-BAND) PARAMETERIZATIONS OF THE EM BIAS

Authors	Normalized EM Bias Parameterization	Theoretical or Observational Basis
1) Jackson [9]	$\beta = -\lambda_3/4$	Gram-Charlier series expression of the joint height-slope pdf using Longuet-Higgins [52] representation of one-dimensional random wavefields and a Phillips [29] saturated spectrum
2) Parsons and Miller [25]	$\beta = -0.00072 - 0.151 * \lambda_3 + 0.0073 * \lambda_3^2$	Ku band laboratory experiment
3) Srokosz [13] Barrick and Lipa [14]	$\beta = -\gamma/8$	Extension of Jackson [9] model to two-dimensional random wavefields
4) Huang <i>et al.</i> [26]	$\beta = F(\xi)$ to first order in ξ : $\beta = -\pi\xi$	Representation of the wavefield in terms of third order "Stokes" waves with a fixed wavelength and random amplitude and phase
5) Glazman and Pilorz [5]	$\beta = -A * (C_o/U)^{-B}$ A and B empirical constants	Evaluation of γ as a function of C_o/U for a generalized power law form of the wavenumber spectrum for equilibrium sea state [18]
6) Glazman and Srokosz [18] Fu and Glazman [19]	$\beta = -C * (\xi/\xi_m)^{-D}$ $\beta = -E * (g * SWH/U^2)^{-F}$ From GEOSAT: $C = 0.013, D = +0.88$ $E = 0.0097, F = +0.55$	C_o/U in (5) expressed in terms of pseudowave age or nondimensional waveheight through JONSWAP (Hasselmann <i>et al.</i> [17]) empirical relationship. C, D, E, and F are empirical constants
7) Choy <i>et al.</i> [45]	$\beta = -0.0115 - 0.0029 * U$	Regression analysis of airborne 10 GHz data
8) Melville <i>et al.</i> [12]	$\beta = -0.0179 - 0.0025 * U$ $\beta = -0.0146 - 0.0021 * U - 0.00389 * SWH$ $\beta = -0.0163 - 2.15/\sigma_o^2 - 0.00291 * SWH$ $\beta = -0.0146 - 0.0036 * U + 0.000073 * U^2$	Ku-band off-shore tower measurements
9) Stewart [23]	$\beta = (-0.03 + 0.00062 * f)(1 \pm 0.5)$ $\beta = -0.0110 - 0.0014 * U$	Collection of airborne data Regression at Ku-band
10) Walsh <i>et al.</i> [7]	$\beta = -0.0030 - 0.0036 * U + 0.00011 * U^2$	Proposed interim algorithm for TOPEX at Ku-band
11) Walsh [42]	$\beta = -0.0066 - 0.0015 * U$	Regression analysis of GEOSAT data
12) Ray and Koblinsky [44]	$\beta = a + b * SWH + c * U + d * \rho + e * SWH^2 + f * U^2 + g * \rho^2 + i * SWH * U + j * U * \rho + k * SWH * \rho$ a, b, c, d, e, f, g, i, j, k: required constants	
13) TOPEX specification [22]		

Notations: β : Normalized EM bias = EM bias/SWH
SWH: Significant wave height in m
U: Wind speed in $m \cdot s^{-1}$
 C_o : Phase speed of the dominant waves in $m \cdot s^{-1}$
 l_o : Wavelength of the dominant waves in m
 λ_3 : Waveheight skewness
 γ : Cross skewness of waveheight and wave slope
 ξ : Significant slope = $SWH/4 * l_o$
f: Radar frequency in GHz
 ξ : Pseudo wave-age
 ξ_m : World average pseudo wave-age value
 ρ : $cst * U/(SWH^{1/2})$

Table I) seems to be the most defensible considering microwave scattering theory, but γ is a complicated combination of second- and third-order statistical moments of the joint wave height and wave slope pdf [13]–[16], which are usually obtained from sea-surface wavenumber spectral models. Since wavenumber spectra are not measured by altimeters, this approach will require input from other sensors and so it is not likely to be used as primary data reduction algorithm. A wave-age dependence has been proposed [5] (formula (5) in Table I), and for a power-law form of the wavenumber spectrum [17], [18] it can be expressed in terms of a pseudo-wave-age value or in terms of nondimensional significant wave height $g * SWH/U^2$ [19]–[21] (expression (6) in Table I). Younger seas are expected to yield higher bias than older seas. The nondimensional significant wave height model could be

used as a primary data reduction algorithm since altimeters provide measures of U and SWH; however, the coefficients need to be checked to establish their range of validity. Finally, the TOPEX team selected the relation given by expression (13) in Table I [22]. Equation (13) contains variables which are known to be highly correlated and thus not independent. Furthermore, they do not use nondimensional parameters which have been found to be useful and robust for characterizing the sea surface.

The reader should be aware that EM bias is a function of 1) microwave wavelength, and 2) the height of the radar above the water surface [7], [8], [23]. While these effects are important, they are beyond the scope of this investigation since as in many other studies, we consider only a single radar frequency and one experimental configuration. Indeed, field measurements from towers differ

from aircraft and satellite measurements so a more general representation will be required to provide an unified model. The data from laboratory experiments may be useful to extend the range of values for validation of models that include range effects.

The feasibility of bias measurements in a laboratory wind-wave tank was demonstrated by Lifermann *et al.* [24]. Parsons and Miller [25] measured the bias from various combinations of wind and mechanically generated waves in the NASA Wallops Flight Facility wind-wave tank using a focused beam radar. Their data from wind cases showed agreement with models by Jackson [9] and Huang *et al.* [26], but the influence of background waves was unexplained.

In this paper, we examine some empirical models for EM bias using new data from experiments that we conducted with a 13.5 GHz *Ku*-band radar in a large wind-wave tank. This microwave frequency is close to one of the TOPEX/POSEIDON altimeter frequencies. These new data and existing data are used in the continuing search for a robust model. The experimental setup and data processing procedures are described in Section II. Section III documents the observational conditions. We present the radar measured wave height distributions in Section IV and modeling results in Section V. In the final section, we discuss the implications of these laboratory experiments for ocean altimetry.

II. EXPERIMENTAL ARRANGEMENT AND DATA PROCESSING PROCEDURES

The experiments were conducted in the large air-sea interaction simulation facility of the IMST Laboratory (Fig. 1), which is described in detail in [27]. The water tank is 40 m long, 3 m wide, and approximately 1 m deep, and the height of the aerodynamical flow above the water surface is about 1.5 m. Waves in the frequency range 1–2 Hz with various steepness up to wavebreaking can also be generated by a completely immersed electrohydraulic wavemaker.

The wind velocity can be adjusted from 0.5 to 14 $\text{m}\cdot\text{s}^{-1}$. We measured the mean wind speed at 1 m above the water surface with a Pitot tube with a precision of a few $\text{cm}\cdot\text{s}^{-1}$. For the range of wind speed considered in this work, the air turbulent boundary layer thickness remains smaller than about 50 cm [28], so the reference velocity U measured at 1 m height represents U_∞ . As usual, when relating laboratory and field observations, the U value is taken as equivalent to U_{10} from field measurements [17], [29]. While the drag coefficient over wind waves is still an open question, the above consideration leads to comparable values of $C_{10} = (u^*/U_{10})^2$ for field experiments and $C = (u^*/U_\infty)^2$ for tank experiments.

A. Experimental Setup

We operated a focused beam, bistatic, 13.5 GHz radar system in the IMST wave tank at a fetch of 28 m, as shown in Fig. 2. The bistatic configuration is similar to a nadir-looking monostatic configuration because in both cases the specular points are the zero slope facets of the water-

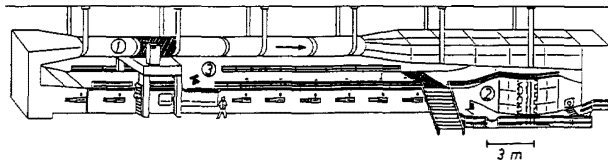


Fig. 1. Schematic view of the IMST large wind-wave facility. 1: fan, 2: electrohydraulic wavemaker, 3: radar device.

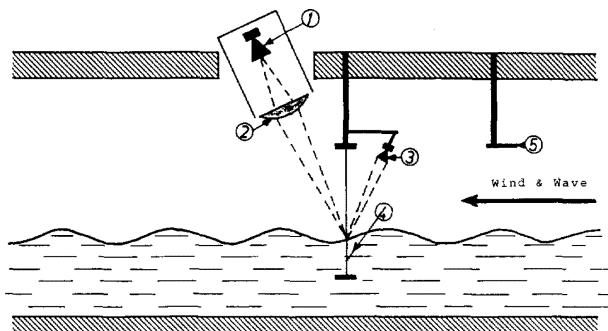


Fig. 2. Side view in the vertical plan of the measuring equipment. 1: radar transmitter, 2: dielectric lens, 3: radar receiver, 4: capacitance wire gauge, 5: pitot tube.

waves. This radar system evolved from a scatterometer system, which was developed by Bliven and Norcross [30] and which has been used in wave-tanks by Giovanangeli *et al.* [31] and Bliven and Giovanangeli [32]. The 1 kHz square-wave modulated source is from a Gunn oscillator, which is attached to a 10° standard gain horn that is aimed at a large focusing lens. The modulated signal is scattered from the water surface and detected by a square-law crystal diode that is attached to another 10° standard gain horn. The signal is amplified and demodulated by two narrow-band HP-415E SWR meters, which were calibrated with a signal generator of known amplitude. The two amplifiers are used in a parallel configuration with gains of 10 and 20 dB, which provides good precision for both low and high signals.

An important consideration for laboratory, tower, and aircraft EM bias studies is to have the radar illuminated spot size much smaller than the length of the dominant waves because we need to know the scattered power level as a function of long wave elevation. So to focus the radio waves, we used a 42 cm diameter dielectric lens, which produces a spot size of 3 cm diameter at the 1 m focal length. This lens was designed and constructed by Parsons and Miller [25].

At first glance, this bistatic configuration is equivalent to a nadir-looking monostatic configuration because in both cases specular points are the zero slope facets. The situation, however, is compounded by the proximity to the surface. The distance between the transmit horn and the lens is 1 m. The distance between the water level at rest and the receive horn is 0.7 m. The energy coming from the standard gain horn is focused by the 42 cm diameter lens to essentially a point at a distance of 1 m from

the lens. Therefore, energy is converging on that point from directions spanning $\pm 12^\circ$; which suggests that specular facets contributing to the received energy will have orientations between $\pm 12^\circ$ of horizontal. But the actual distribution includes the weighting function from the source 10° standard gain horn, which has a relatively narrow beamwidth, i.e., a -3 dB attenuation at $+5^\circ$ and -5° and a -10 dB attenuation at -8° and $+8^\circ$. The two sidelobes are centered around -14° and $+14^\circ$ and their relative level is -15 dB. So they do not contribute to illuminate the spot. Consequently, the wave tank specular facets are predominantly from within $\pm 5^\circ$ of horizontal. The reader should be aware that this differs somewhat from the altimeter case where essentially horizontal facets contribute. Details on the lens design and on properties of the focused apertures can be found in [33]. Installation and performance of a radar focused by the lens used in this study is described in [34] and [35].

The radar functioned as a scatterometer because it measured reflected power but not range. Therefore, the water elevation was measured with a capacitance probe of 0.3 mm outer diameter located within the radar spot. Consequently *backscattered power and water surface level signals were acquired simultaneously at the same location, thus allowing EM bias evaluations*. The accuracy of the water level measurements by the probe was ± 0.2 mm. Test runs made with and without the wave gauge showed that the reflected power was decreased by less than 1% when the probe was present within the radar spot, but this decrease was not water level dependent, and consequently did not affect EM bias determination.

Radar absorbing material was installed at appropriate locations around and above the radar setup, on the ceiling, and on the side walls of the tank in order to minimize multipath reflection. Numerous tests made with the same environmental conditions but with different configurations of absorbing material showed that EM bias determination was insensitive to the placement of absorbing material. This is probably because the received power from multipath reflections was much lower than from specular facets. Overall, the signal-to-noise ratio was found to be excellent: a small disk of absorbing material just above the spot decreased the reflected power by more than 30 dB.

B. Radar Calibration

To compute EM bias, only reflectivity measurements are needed—so absolute calibration of the radar system is unnecessary. We defined a *reflectivity signal* as the ratio between the power reflected from the roughen surface to the corresponding flat surface. A range scaling factor is needed since measurements showed that the backscattered power from a calm water surface is a function of water level elevation (range effects and spot size variations). There is also an interference effect: radio waves going back and forth along the path between the transmitter, the lens, the water surface, and the receiver produce stationary electromagnetic waves with nodes and antinodes at

half wavelength intervals. The interference effect is significantly reduced by the bistatic configuration and by absorbing material placed at appropriate locations [25], [35]. To obtain the reflectivity signal, a range scaling factor must be determined as a function of water level. The easiest way to calibrate was to record the backscattered power while slowly draining or filling the tank with water, which was the procedure used by Parsons and Miller [25]. Thus, for a given tank water level h , the acquired flat surface reflected power $P_{\text{cal}}(h)$ was considered as the basic reference power for calibration, and the *reflectivity signal* is

$$r(t) = P(t)/P_{\text{cal}}(h(t)) \quad (1)$$

with $P(t)$ and $h(t)$ being, respectively, the backscattered power and water elevation at instant t . Kirchner *et al.* [35] found theoretically a radar power return proportional to D^{-2} due to range effects and spot size variations with the lens configuration (D being the distance between the lens and the water level). From the drain tests, we found the backscattered power P to be a decreasing function of D , but the main variations in P were due to interference effects (radio waves going back and forth). The correction factor oscillates every half radar wavelength with approximately a 0.7 dB amplitude. Interferences effects are discussed in detail in [33] and [34]. Measured variations of the scaling factor $P_{\text{cal}}(h)$ were consistent with our assumptions and with the above cited previous studies.

Another concern for simulating satellite conditions by ground based experiments is the so-called *focusing* effect. When operating a radar from space, the facet-like reflectors on the surface that cause the returned signal are nearly horizontal. It is desirable to simulate these conditions from onboard an aircraft, from a tower, or in a wave tank. One potential problem that can arise is due to *focusing* facets that are attributable to the possibility of concave (upward) facets focusing the incident signal back toward the receiver. *Reinforcement*, which may be viewed as a generalized representation of *focusing*, occurs when there is coherent combination of reflection elements distributed across all, or a portion of the footprint. At the surface, such reinforcement is a consequence of favorably oriented plane facets concentric to the illumination wavefront, and having a range distribution that is relatively concentrated with respect to the radar wavelength. These facets will give a high power level at the radar and since these facets will be more predominant in the troughs due their concave shape, there could be a *built-in* bias. While this effect may be important, a complete analysis has not yet appeared in the literature and it is beyond the scope of this study.

We have, however, investigated scattering using a simple geometric ray-tracing model. We simulated the trajectories of optic rays reflected by the water surface using geometric optic approximation. Given an illuminated area, we computed the density of rays that come back to the receiver. The built-in bias due to focusing effect was defined by the mean of the wave profile weighted by this density function. We quantified this bias for cases of sinus waves for which no EM bias should occur due to the crest-

to-trough symmetry. Waves were characterized by their wavenumber k and their steepness $\epsilon = ak$, a being the amplitude. The computations showed that the built-in bias due to focusing was maximum when the radius of curvature above the trough, $r_c = (\epsilon k)^{-1}$, was equal to radar elevation R . The results are summarized in Table II. The parameters of interest are the ratios R/r_c and d/L (d is the diameter footprint, and L is the wavelength: $L = 2\pi/k$). When $R/r_c \gg 1$, there is no focusing effect due to geometric consideration. This is the case for satellite data and some aircraft data. When $R/r_c \sim 1$ the built-in bias is significant when the spot size is not small relatively to the dominant wavelength. This is typical of patterns seen on the bottom of illuminated swimming pools, and this could occur in wave-tanks for laboratory radar systems without a lens to focus the electromagnetic waves. When $R/r_c \sim 1$ and $d/L \ll 1$, which is the normal situation for wave-tank with focused radar systems, tower, and some aircraft data, the focusing effect is relatively small: the built-in bias is of order 0%-2%, depending upon R , L and the wave steepness ϵ .

This simple model does not solve the full focusing problem, but it gives some clues. An analytical approach of the focusing question is not feasible because the surface is unknown. If the surface characteristics were known, the EM bias issue would be completely solved. Generalized focusing is determined by spatial coherence of the collective facet reflections. The fundamental spatial scale parameter is not the footprint diameter, but the effective diameter of the coherent footprint. The relative coherent scattering component may differ depending upon radar range and radar wavelength. A broad set of data from wave-tanks, towers, and aircraft will be useful to validate more precise physical models of focusing effects and the data presented herein can contribute to those efforts.

C. Data Processing Procedures

For each run, the two analog 10 and 20 dB gain radar outputs and the wave gauge analog signal were acquired at 300 Hz. The analog signals were low-pass filtered with a cut off frequency of 100 Hz in order to avoid aliasing. 180 000 samples per line and per run were stored in memory, so each run lasted 10 minutes. Data were acquired both on a PC 386 for real time analysis and on a HP 1000 computer for post processing. The 10 and 20 dB gain radar signals were combined to yield double-decade high-precision backscattered power signals $P(t)$, and the reflectivity signals $r(t)$ defined in (1) were computed.

Probability density functions (pdf) of wave height elevation were estimated in a standard manner from the wave gauge signal. Elevation data were normalized by the standard deviation of the wave height distribution. Then the normalized values were sorted into elevation bins of width $1/15$ standard deviation. The pdf value of bin number “ i ” was equal to the ratio of the number of samples that belonged to this bin, namely N_i , to the total number

TABLE II
BUILT-IN BIAS DUE TO GEOMETRIC CONSIDERATIONS

	$R/r_c \sim 1$	$R/r_c \gg 1$
$d/L \ll 1$	$\sim [0\% \ 2\%]$ (Laboratory focused radar)	0% (aircraft)
$d/L \sim 1$	$\sim 20\%$ (Laboratory not focused radar)	0% (aircraft)
$d/L \gg 1$	$\sim 20\%$ (Bottom of illuminated swimming pool)	0% (satellite)

Notations L : Surface wavelength
 d : Diameter footprint
 R : Radar range
 r_c : Radius of curvature of the illuminated facet

of data samples:

$$\text{pdf}_{\text{Height}}(i) = N_i / \sum_k N_k. \quad (2)$$

In order to compute the elevation pdf of the facets that reflect the radio waves, each sample was weighed by its reflectivity value. So for each elevation bin, the *pdf of radar elevation value* was equal to the amount of reflectivity produced by the samples that belong to that bin, normalized by the total reflectivity. If r_{ij} is the reflectivity of sample j of bin i , then

$$\text{pdf}_{\text{Radar Height}}(i) = \sum_j r_{ij} / \sum_k \sum_n r_{kn}. \quad (3)$$

The EM bias is just the difference between the means of distributions (2) and (3):

$$\text{EM bias} = \sum_i h_i (\text{pdf}_{\text{Radar Height}}(i) - \text{pdf}_{\text{Height}}(i)). \quad (4)$$

For each test run, we computed distributions (2) and (3) and compared their first four moments. The significant wave height, SWH , was taken as four times the standard deviation. FFT analysis gave us the dominant frequency n_o of the energy containing the waves. The dominant wavelength l_o of the wave field was obtained from n_o using the linear dispersion relation for deep water gravity waves. We calculated also the significant slope ξ , $\xi = SWH/4 * l_o$, the phase speed of the dominant waves C_o , $C_o = l_o * n_o$, and the mean r_o of the reflectivity coefficient r_{ij} .

III. OBSERVATIONAL CONDITIONS

Our goal was to cover the whole set of experimental conditions allowed by the IMST facility. Consequently, 83 different experiments have been conducted and were scheduled as follows:

- 1) 22 wind runs with wind speed ranging from 0 to 14 $\text{m} \cdot \text{s}^{-1}$.
- 2) 19 runs with paddle generated waves: the first 10 with a paddle frequency of 1.75 Hz but with different paddle amplitudes and the last 9 with the same wave ampli-

tude but with paddle frequencies ranging from 1.1 to 2.1 Hz. The significant slope ξ ranged from 0.002 to 0.014.

3) 42 runs with both wind waves and paddle generated waves:

- paddle frequency 1.1 Hz, $\xi = 0.008$, U ranging from 0 to $10 \text{ m}\cdot\text{s}^{-1}$ (10 runs)
- paddle frequency 1.3 Hz, $\xi = 0.007$, U ranging from 0 to $11 \text{ m}\cdot\text{s}^{-1}$ (11 runs)
- paddle frequency 1.75 Hz, $\xi = 0.002$, U ranging from 0 to $11 \text{ m}\cdot\text{s}^{-1}$ (11 runs)
- paddle frequency 1.75 Hz, $\xi = 0.014$, U ranging from 0 to $11 \text{ m}\cdot\text{s}^{-1}$ (10 runs)

Measurements were made at a fetch of 28 m. At this distance, the wave field was free from reflection from the wave absorber located at the downwind end of the tank. In the next section, we describe some illustrative results concerning the radar and wave height signatures related with the EM bias determination.

IV. RADAR SIGNALS AND WAVE HEIGHT DISTRIBUTIONS

A. Time Series

Fig. 3 displays time series of the water surface elevation $h(t)$ and the radar reflectivity $r(t)$ for different wind speeds. With the water surface at rest, both signals are flat. At $U = 1.7 \text{ m}\cdot\text{s}^{-1}$, the radar signal is still quite flat as the wavelength of the dominant capillarity-gravity waves ($\lambda_0 = 5 \text{ cm}$) is shorter than three times the 2.2 cm radar wavelength [36]. At $U = 2.7 \text{ m}\cdot\text{s}^{-1}$, the wavelength of the dominant waves is 14 cm and the radar signal changes drastically. Significant oscillations appear at the frequency of the dominant waves. The reflected power is much higher over the wave troughs than over the wave crests. This asymmetry, which characterizes the bias, is even more noticeable at $U = 4.0 \text{ m}\cdot\text{s}^{-1}$. As the wind speed increases, the average value of the backscattered signal decreases and the crest-to-trough asymmetry increases. At $U = 11.0 \text{ m}\cdot\text{s}^{-1}$ the radar signal appears to be dominated by peaks occurring ahead of near breaking crests. This has been already observed by Lifermann *et al.* [24] under similar environmental conditions. The peaks are probably due to the flat surface that exists ahead of a near breaking crest, as identified by Bonmarin [37] using video techniques. Note that there is no backscattering at nadir of the breaking crests.

For moderate winds (wind speed ranging from 3 to $8 \text{ m}\cdot\text{s}^{-1}$), the radar is also sensitive to the water wave natural modulations: on the average, the reflected power is smaller over groups of steep waves than between wave groups. The observed low-frequency variation in the backscattered power is due to local changes in the slope variance produced by subharmonic wave instabilities.

For cases of mechanically generated waves with no wind forcing, the water surface elevation $h(t)$ and the associated radar signal $r(t)$ are shown on Figs. 4 and 5. For small steepness ($\xi = 0.007$ —Fig. 4), the radar signal is periodic with a high peak over each wave trough and a

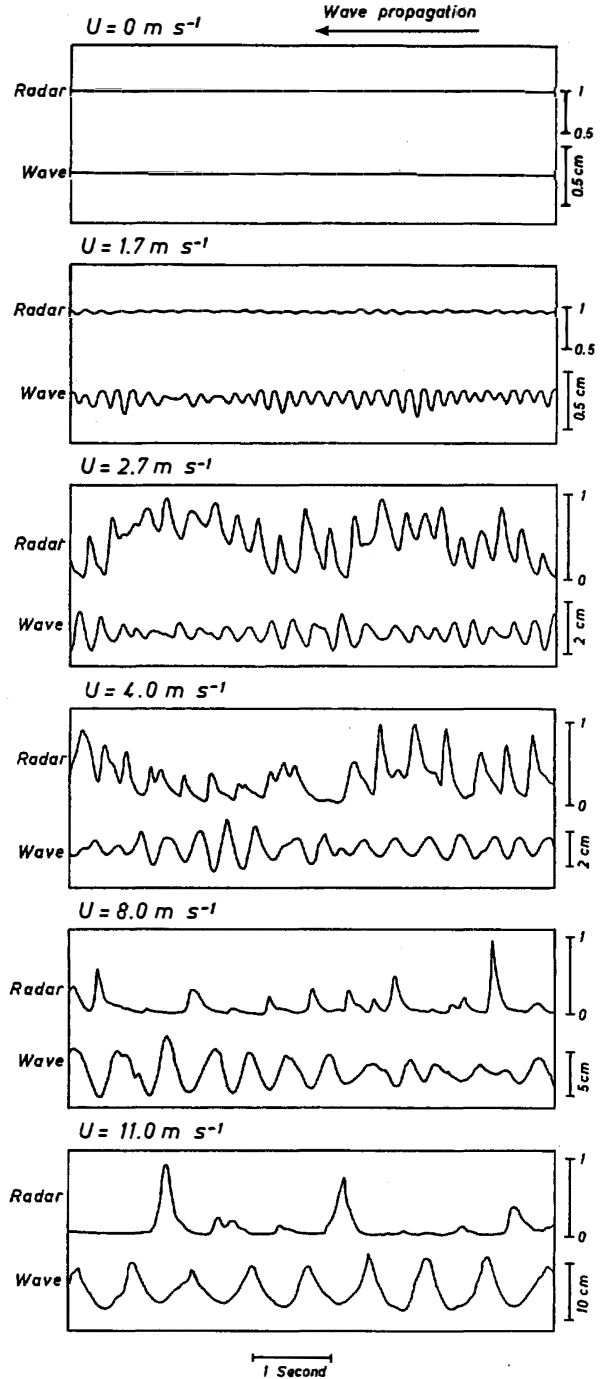


Fig. 3. Samples of time series of the water surface deflection level $h(t)$ and the radar reflectivity signal $r(t)$ for pure wind waves.

low peak above each wave crest, thus leading to a negative EM bias ($\beta = -2.7\%$). This differs from the Parsons and Miller results [25] for which positive bias was reported for paddle waves. Theoretically, the bias should be zero for a sinus wave because the mean level of the horizontal facets is zero, but for Stokes waves the bias is

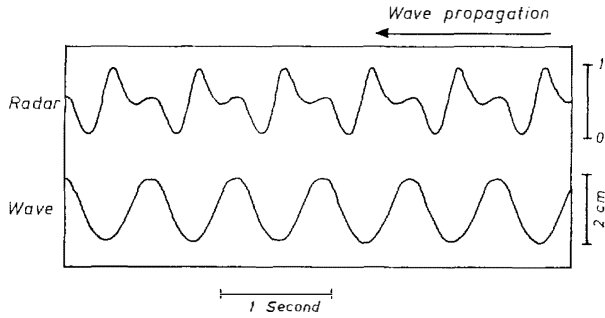


Fig. 4. Samples of time series of the water surface deflection level $h(t)$ and the radar reflectivity signal $r(t)$ for mechanical wave at 1.3 Hz frequency and small steepness ($\xi = 0.007$).

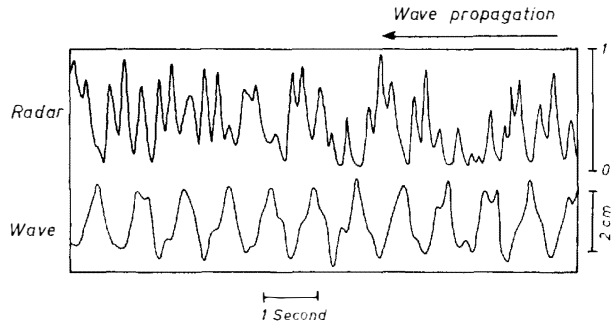


Fig. 6. Samples of time series of the water surface deflection level $h(t)$ and the radar reflectivity signal $r(t)$ for case of mechanical wave at 1.3 Hz frequency and small steepness ($\xi = 0.007$) with wind effect ($U = 2.7 \text{ m}\cdot\text{s}^{-1}$).

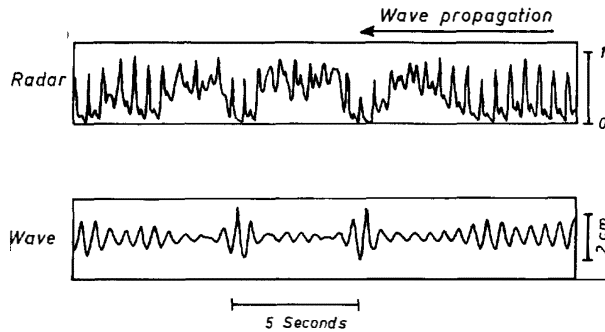


Fig. 5. Samples of time series of the water surface deflection level $h(t)$ and the radar reflectivity signal $r(t)$ for mechanical wave at 1.75 Hz frequency and moderate steepness ($\xi = 0.012$).

of order $-\pi * \xi$ [26], i.e., -2.2% . For large steepness ($\xi = 0.012$ —Fig. 5), time series of wave elevation show clearly the presence of wave groups due to natural subharmonic instabilities. The amount of reflected power increases significantly between two wave groups thus leading to low frequency modulations of the radar signal, and there is a radar enhancement above each wave trough thus giving a significant negative EM bias ($\beta = -5.5\%$).

An example of a combination of wind waves and paddle waves is shown on Fig. 6. In this case, a light wind ($U = 2.7 \text{ m}\cdot\text{s}^{-1}$) is acting on the gentle paddle waves described in Fig. 4. If compared with this previous case, the radar response changes drastically with no evident periodicity due to the presence of small ripples. The effect of the light wind is to decrease the bias ($\beta = -1.6\%$) probably because the wind produces more uniform roughness along the paddle waves. Then, when we increase the wind speed above such paddle waves, we find the EM bias to be an increasing function of wind speed as it is the case for pure wind waves. Time series of mixed waves conditions are quite difficult to interpret because there is no obvious way to separate the backscattering due to wind waves from the backscattering due to paddle waves. Non-linear interactions between waves at different scales are likely to occur and how they affect the probability density functions is of crucial interest here.

B. Probability Density Functions

Fig. 7 displays the pdf of the *actual* and the *radar observed* wave-height distributions as defined in Section II-C, for various observational conditions of pure wind waves. Some features are of interest. For example, both wave and radar distributions depart from Gaussian distributions, and as the wind speed increases, the asymmetry increases. Also the two pdf depart more and more from each other, the radar pdf being more asymmetrical than the wave-height pdf. Lastly, at $U = 14 \text{ m}\cdot\text{s}^{-1}$, the right side of the wave-height pdf exhibits a small bump, known to be due to wavebreaking [38]. Such a bump does not appear on the radar pdf, which suggests that the crests of breaking waves are not significant scattering sources for altimetry.

Moments up to order four were computed from these distributions. EM bias values, which are related to the mean values of the distributions, will be presented in the next section. Results on SWH, computed from second-order moments of both the wave height and the radar pdf are compared on Fig. 8(a). There is a systematic bias between the SWH observed by the radar and the actual SWH. Radar computed SWH is approximately 90% of the actual SWH. This is in accordance with recent results, namely, the GEOSAT measured SWH appeared generally smaller than the SWH values delivered by buoys [11], [39] and wave models [40].

The skewnesses of the wave height and the radar distributions displayed in Fig. 7, are compared on Fig. 8(b). For values smaller than 0.3, the skewnesses are identical. But at higher values, the radar skewness is almost three times greater than the actual wave height skewness. This is important with regard to the oceanic remote sensing of the wave height skewness [2], [10]. Indeed, no difference is usually made between the skewness of the specular facets distribution and the actual wave height skewness. For wind generated waves, at short fetches the two skewnesses clearly depart significantly from each other. No specific relationship was found between the kurtosis of the two distributions.

Examples of pdf corresponding to mixed wind waves and paddle waves are shown on Fig. 9. Pure mechanical

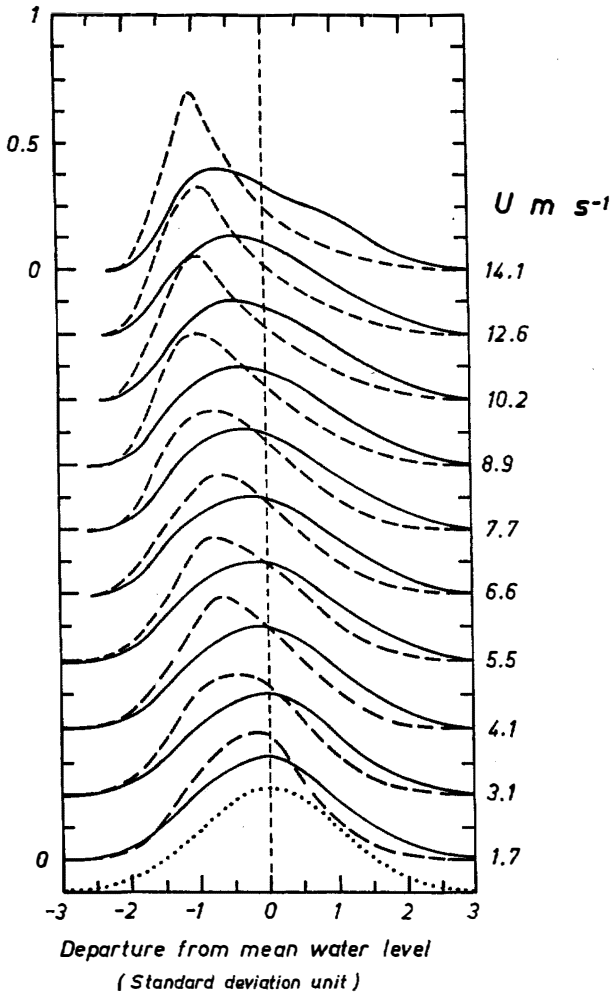


Fig. 7. Probability density functions of the wave-height (—) and the radar observed wave-height (---) as defined in Section II-C for wind waves for wind speed ranging from 1.7 to 14.1 $\text{m}\cdot\text{s}^{-1}$. (.....) normal distribution.

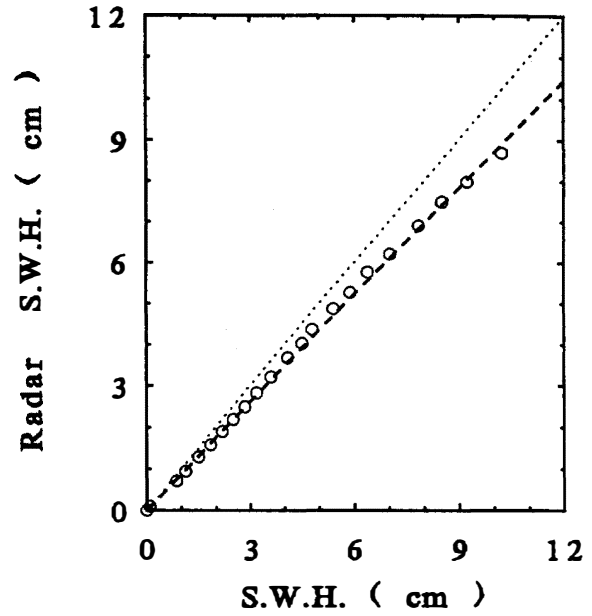
waves are characterized by bimodal distributions, but as the wind speed increases, the wave field evolves towards unimodal distributions. The bimodal distribution disappears completely at $U = 11 \text{ m}\cdot\text{s}^{-1}$. All the distributions are far from being Gaussian. The skewnesses of the radar distributions are significant for U greater than $2.7 \text{ m}\cdot\text{s}^{-1}$. For each test, the reflectivity is on average much higher near the troughs than near the crests of the waves, thus yielding negative values of the bias.

V. EM BIAS RESULTS

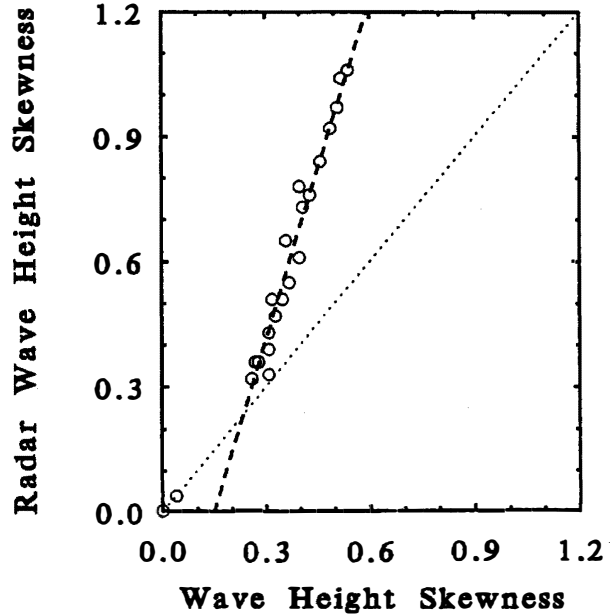
A. Statistics

For each run, we computed the EM bias as indicated in Section II-C.

Table III summarizes the mean and the standard deviation of the EM bias data, considering successively the 22 wind runs, the 19 paddle runs, the 42 runs with mixed sea



(a)



(b)

Fig. 8. (a) Comparison between the true significant wave-height and the radar observed significant wave-height. (--- : $y = 0.87 * x$). (b) Comparison between the true wave-height skewness and the radar observed wave-height skewness. (--- : $y = 2.7 * x - 0.4$).

conditions, and then the whole set of the 83 runs. The overall mean value of the EM bias is of order -3 mm . Bias values are always negative except for the wind run with a very light wind velocity of $U = 1.7 \text{ m}\cdot\text{s}^{-1}$. In this case the bias was very close to zero with a value of $+0.12\%$ of SWH. Table III indicates that, on the average, paddle waves generate much smaller biases than wind

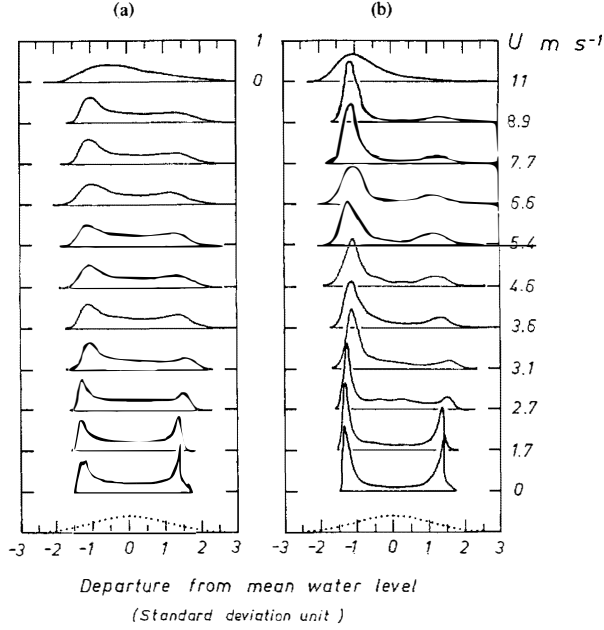


Fig. 9. Probability density functions of: (a) wave-height and, (b) radar observed wave-height. Case of mechanical wave at 1.3 Hz frequency and small initial steepness with wind effect (variable wind speed U as indicated). (.....) normal distribution.

TABLE III
STATISTICAL VALUES OF THE EM BIAS

Bias	Runs	Wind Waves (22 runs)	Paddle Waves (19 runs)	Mixed Waves (42 runs)	Whole Data Set (83 runs)
EM Bias Mean value (cm)		-0.53	-0.13	-0.32	-0.33
EM Bias Standard deviation (cm)		0.45	0.06	0.29	0.34
β Mean value (% SWH)		-9.9	-4.7	-6.5	-7.0
β Standard deviation (% SWH)		4.1	1.1	3.2	3.6

waves or mixed waves. The scatter of the data is quite large. The standard deviations are as high as the mean values.

From Table III, the bias as a percentage of SWH possesses a mean value of order -7.0% . This is significantly higher than values usually found in open oceans in Ku -band domain (-2% to -5% of SWH) [7], [12]. Reasons for such difference will follow. It is seen that pure wind waves yield, on the average, values about 52% higher than the values corresponding to mixed waves and about 110% higher than the values corresponding to pure paddle waves. This is qualitatively consistent with the numerical work of Ioualalen *et al.* [41], who found higher biases for three dimensional wavefield than for two dimensional

waves. The extreme value, $\beta = -15\%$, was obtained when the wind speed was maximum ($U = 14 \text{ m}\cdot\text{s}^{-1}$). Clearly, a constant value is not appropriate for characterizing the bias.

B. Parameterization with the Wind Speed and the Significant Wave Height

In order to understand the bias sea-state dependence, we have made regression analyses between absolute EM bias values and some other parameters such as SWH, U , ξ , skewness, l_o , n_o , r_o , as defined in Section II-C. We found quite good correlations with wind speed ($r^2 = 0.78$), significant slope ($r^2 = 0.71$) and skewness ($r^2 =$

0.52), but not with dominant wavelength or dominant frequency (r^2 lower than 0.2). However, the best correlation was between EM bias and significant wave height. The relationship between these two parameters is not linear but quadratic (Fig. 10):

$$\begin{aligned} \text{EM bias} = & +0.014 - 0.034 * \text{SWH} \\ & - 0.011 * \text{SWH}^2 \quad r^2 = 0.87 \quad (5) \end{aligned}$$

(with EM bias and SWH in cm)

Because the absolute EM bias is so clearly related with SWH, we have focused our attention on the so-called *normalized* or *non-dimensional* EM bias ratio $\beta = \text{EM bias} / \text{SWH}$. Considering all the 83 runs, we found a better correlation between β and U ($r^2 = 0.74$) than between β and SWH ($r^2 = 0.53$). Fig. 11 shows clearly the wind speed dependence of the normalized EM bias. Taking into account runs with nonzero wind speed, we found the following relationship:

$$\beta = -0.0190 - 0.0100 * U \quad r^2 = 0.77 \quad (6)$$

(with U in $\text{m} \cdot \text{s}^{-1}$)

Quadratic relationships between absolute EM bias and significant wave height as well linear relationships between normalized EM bias and wind speed have also been observed in open seas by various authors (see Table I, and [7], [12] for a review).

Note that if we consider only the pure wind wave runs, a mean square regression analysis conducted with a parabolic representation produces a high correlation coefficient (Fig. 11):

$$\begin{aligned} \beta = & +0.00113 - 0.0208 * U + 0.00074 * U^2 \\ r^2 = & 0.92 \quad (7) \end{aligned}$$

(with U in $\text{m} \cdot \text{s}^{-1}$)

This parabolic expression suggests a saturation effect at high wind speed with a maximum EM bias occurring at $U = 14 \text{ m} \cdot \text{s}^{-1}$. From the wind run data of Parsons and Miller [25], we found a saturation effect occurring at $U = 18 \text{ m} \cdot \text{s}^{-1}$. This saturation effect has been mentioned in [23] (expression (9) in Table I), from the Melville *et al.* [12] open field tower measurements, the maximum bias occurring at $U = 25 \text{ m} \cdot \text{s}^{-1}$. Also reported is the Ku -band parabolic expression proposed by Walsh [42] as an interim algorithm for the TOPEX mission, the maximum bias occurring at $U = 16 \text{ m} \cdot \text{s}^{-1}$ (expression (11) in Table I). Recently, Rodriguez *et al.* [8] have numerically predicted that the bias would increase with wind speed up to about $U = 10 \text{ m} \cdot \text{s}^{-1}$ then it would decrease with increasing wind speed. Analyzing GEOSAT altimeter data, for wind speeds above $10 \text{ m} \cdot \text{s}^{-1}$ and SWH greater than 4 m, Witter and Chelton [43] found that biases decreased with increasing wind speed, which they attributed to effects of satellite pointing attitude angle and sea state.

The various parameterizations relating β to the wind velocity U , listed on Table I, need clearly to be compared and discussed. The coefficients from our laboratory data are significantly higher than those of the expressions es-

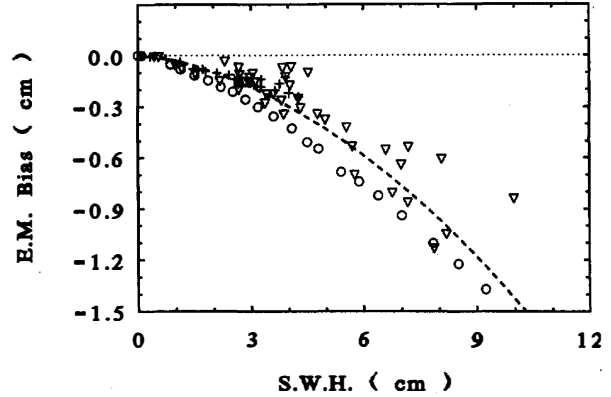


Fig. 10. Absolute EM bias as a function of significant wave-height (○) wind waves, (+) paddle waves, (∇) mixed waves. (---) EM bias (cm) = $0.014 - 0.034 * \text{SWH} - 0.011 * \text{SWH}^2$, $r^2 = 0.87$ (SWH in cm).

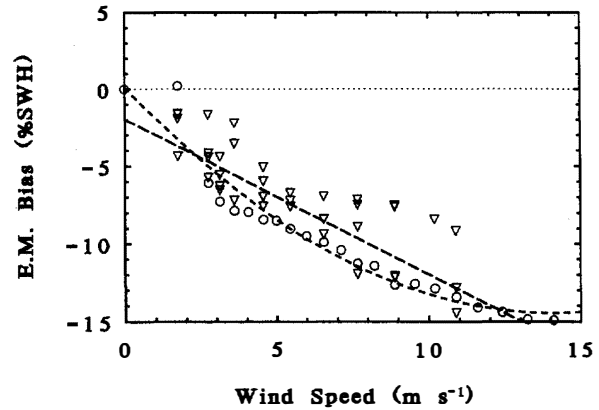


Fig. 11. Normalized EM bias as a function of wind speed. (○) wind waves, (∇) mixed waves. (—) $\beta = -0.0190 - 0.0100 * U$, $r^2 = 0.77$ (---) $\beta = +0.00113 - 0.02086 * U + 0.00074 * U^2$, ($r^2 = 0.92$, wind waves) (U in $\text{m} \cdot \text{s}^{-1}$).

established from field measurements, however, the proposed coefficients change from one expression to another in an erratic way. Clearly no universal parameterization of the form $\beta = a + b * U + c * U^2$ can be proposed at this time. Specification of the a , b and c coefficients as a function of environmental conditions remains an open problem. Walsh *et al.* [7] suggested that part of the differences may be due to differences in the experimental setup. Influence of the radar altitude above the sea surface was called forth: the lower the altitude the higher the bias due to microwave focusing by the sea surface waves, as discussed in Section II-C. Recently, Stewart [23] suggested that surfactants would affect EM bias determination.

Observations from a large variety of conditions led us to think that the required coefficients a , b and c would be themselves sea-state dependent. The expressions give only explicit dependence of β on wind velocity U . We note, however, that at the same wind speed U , the wavefield from different experiments may greatly differ from each other depending upon the fetch, the water depth, the pres-

sure of currents or swell, etc. As a consequence, the biases would differ from each other. Note that the results of [44] (expression (12) in Table I) addressed mainly to deep ocean while those of [12] (expressions (8) and (9) in Table I) were obtained in shallow water area, and that IMST wave-tank results came from young waves on deep water. Clearly, additional parameters related to the sea-state need to be introduced.

In that respect Melville *et al.* [12] chose SWH, a parameter directly available from altimeter measurements. They proposed the following expression,

$$\beta = -0.0146 - 0.0021 * U - 0.0039 * SWH$$

$$r^2 = 0.74$$

with the same correlation coefficient, IMST data fit with the expression:

$$\beta = -0.032 - 0.0073 * U - 0.1423 * SWH$$

$$r^2 = 0.74 \quad (8)$$

In these formulas U is in $m \cdot s^{-1}$ and SWH in m.

Again the coefficients greatly differ from one expression to the other. More particularly the SWH coefficients are not the same order of magnitude because tank-generated wave heights and open-sea wave heights are not the same order of magnitude. These later formulas involving SWH would have the same disadvantage as the previous formulas relating β to U , that is they apply only for particular observational conditions.

C. Representation with Dimensionless Parameters

There exists at this time no fully satisfactory theoretical way to relate the EM bias to the sea-state because it is necessary to predict the joint probability density function of wave-height and wave slope starting from the basic hydrodynamic equations. This is still actually out of reach of the theoretical models of wind waves. However the characterization of the sea-state has progressed quite significantly on the basis of semi-empirical investigations. The sea-state characteristics are known to be better characterized by dimensionless parameters such as $g * SWH / U^2$, $n_o * U / g$, $g * X / U^2$, $g * T / U \dots$ where X is the fetch and T the wind duration. An homogeneous relationship relating β , which is a dimensionless parameter, to the sea-state would involve such parameters. Note that in existing analytical work, the EM bias is related with dimensionless variables such as the wave-height skewness [9], significant slope [26], the height slope cross skewness [13], the wave age and the nondimensional wave height [5], [18], [19].

Fig. 12 displays β versus the wave-height skewness for both airborne 10 GHz data [45] and IMST wind-wave tank 13.5 GHz data. Clearly, there is no gap between the two data sets. In addition, the evolution over the large range of the wave-height skewness is quite well predicted by the Jackson [9] theoretical expression. Unfortunately, from a practical point of view, the skewness cannot be used to predict the bias because the altimeter itself is not

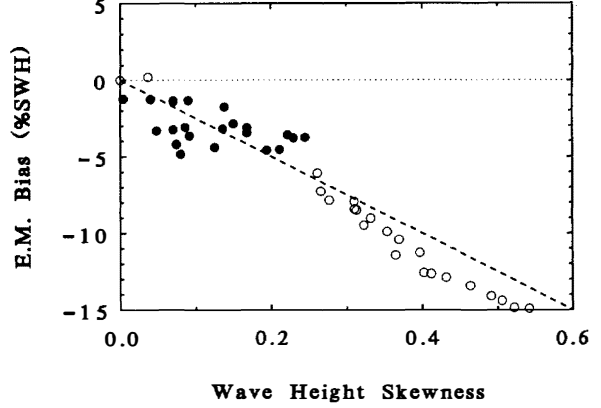


Fig. 12. Normalized EM bias as a function of wave height skewness. (○) laboratory 13.5 GHz data for pure wind waves. (●) Choy *et al.* airborne 10 GHz data [45]. (----) Jackson [9] theory.

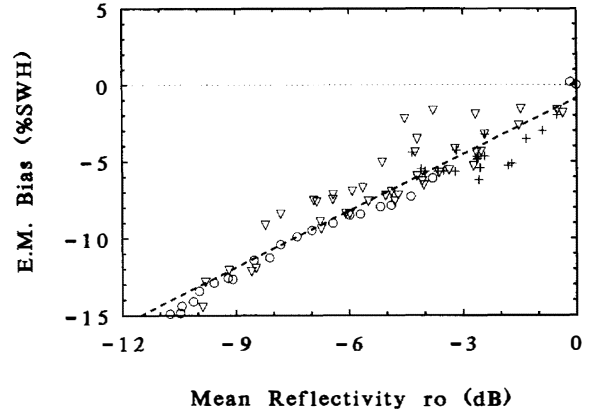


Fig. 13. Normalized EM bias as a function of mean reflectivity r_o , as defined in Section II-C. (○) wind waves, (+) paddle waves, (∇) mixed waves. (----) $\beta = -0.00852 + 0.0123 * r_{o(dB)}$, $r^2 = 0.89$.

able to measure this parameter with enough precision or confidence [10], so other dimensionless parameters are required for the EM bias determination.

The dimensionless mean reflectivity coefficient r_o , defined in Section II-C, is a candidate for the EM bias parameterization because it can be obtained from altimeter data. Theoretically, $r_o \approx 1/\sigma_x^2$ where σ_x^2 is the filtered slope variance, the low-pass cutoff wavelength being the 2.2 cm radar wavelength [36]. Following Cox and Munk [46], $\sigma_x^2 \approx U$. We found previously $\beta \approx U$, so we expected $\beta \approx 1/r_o$. Considering all the nonzero wind velocity runs, we found a good correlation, $r^2 = 0.86$, between β and $1/r_o$. The correlation decreased to $r^2 = 0.73$ if $1/r_o^2$, as proposed by Melville *et al.* [12], is considered instead of $1/r_o$. When the overall set of 83 runs is taken into account, a completely empirical approach yields a highly correlated linear relationship between β and r_o expressed in decibels (Fig. 13):

$$\beta = -0.00852 + 0.0123 * r_{o(dB)} \quad r^2 = 0.89. \quad (9)$$

This is the highest correlation coefficient found between β and another parameter when all the 83 runs are considered all together. The reflectivity coefficient is a good parameter to predict the bias probably because it contains intrinsic information on sea state. Nevertheless, we did not find the inverse square law dependence between the normalized bias and the backscattered power [see Table I, formula (8)] to be the optimal representation.

It is quite well established that the wave age C_o/U , where C_o is the phase speed of the dominant wave, and the nondimensional significant wave-height $g * SWH/U^2$ are two basic quantities which characterize the sea state on statistical grounds. These quantities have also been used to parameterize EM bias.

Fig. 14 displays β versus C_o/U for both the wind-waves runs and the mixed-waves runs. The following regression formula holds:

$$\beta = -0.0168 * (C_o/U)^{-0.85 \pm 0.05} \quad r^2 = 0.92. \quad (10)$$

Note that: 1) the formula agrees with [5] (formula (5) in Table I). Young waves yield higher bias than older waves; 2) data from wind waves fit closely to the regression curve; and 3) the correlation coefficient is relatively high, but large scatter is observed for mixed-waves runs. This is discussed elsewhere.

Fig. 15 is a scatter plot of β versus $g * SWH/U^2$. We found the following least square regression:

$$\beta = -0.0049 * (g * SWH/U^2)^{-0.62 \pm 0.06} \quad r^2 = 0.75 \quad (11)$$

Again, large scatter is observed for mixed-waves runs. Also shown on Fig. 15 are open field measurements from Choy *et al.* [45] at X-band (10 GHz), and Walsh *et al.* [7] at Ku-band (13.6 GHz). In spite of the small differences between the operating frequencies, there is no gap between the different data sets. The relationship (11) slightly underestimates the other data sets, but this kind of representation is certainly more consistent with different sea conditions than a “ β versus U ” or a “ β versus SWH ” relationship. Taking into account both IMST and open field measurements [7], [45] the regression between $g * SWH/U^2$ and β becomes (cf. Fig. 15):

$$\beta = -0.0117 * (g * SWH/U^2)^{-0.42 \pm 0.03} \quad r^2 = 0.80. \quad (12)$$

The average of the exponents of (11) and (12) is about -0.5 . Such an exponent would make the resulting equation linearly proportional to wind speed. It may really be that this parameterization works because it is a surrogate for wind speed, with a randomizing effect from wave height.

A point of interest is that formulas (10) and (11) are quite similar with the Fu and Glazman [19] formulas using *GEOSAT* data and Hasselmann *et al.* [17] like expressions to relate wave age with the dimensionless wave-

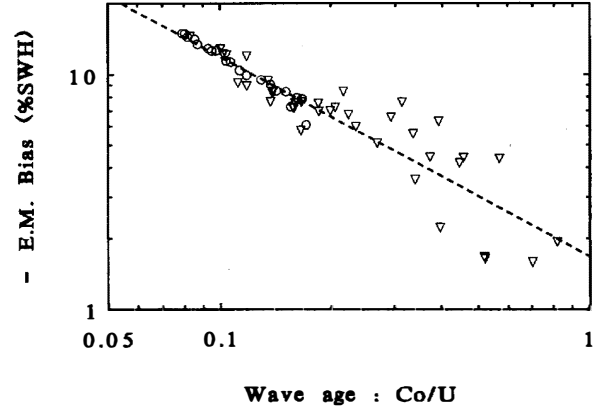


Fig. 14. Normalized EM bias as a function of wave age C_o/U . (\circ) wind waves, (∇) mixed waves. (---) $\beta = -0.0168 * (C_o/U)^{-0.85}$, $r^2 = 0.92$.

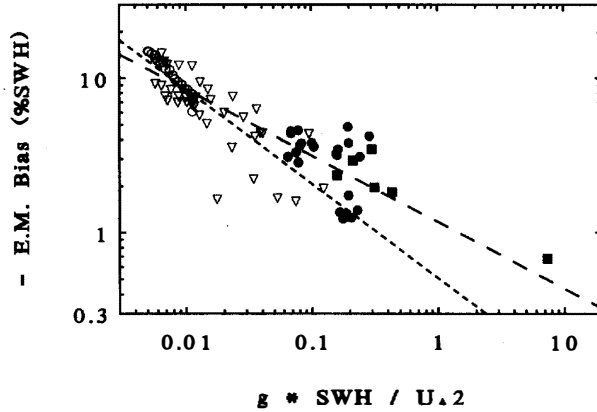


Fig. 15. Normalized EM bias as a function of the dimensionless significant wave-height $g * SWH/U^2$. (\circ) 13.5 GHz data from laboratory wind waves, (∇) 13.5 GHz data from laboratory mixed waves. (\bullet) Choy *et al.* airborne 10 GHz data [45]. (\blacksquare) Walsh *et al.* airborne 13.6 GHz data [7]. (---) $\beta = -0.0049 * (g * SWH/U^2)^{-0.62}$, ($r^2 = 0.75$; IMST data) (---) $\beta = -0.0117 * (g * SWH/U^2)^{-0.42}$, ($r^2 = 0.80$; IMST, Choy and Walsh data).

height. The Fu and Glazman [19] formulas are

$$\beta = -0.013 * (\xi/\xi_m)^{-0.88 \pm 0.37} \quad (13a)$$

$$\beta = -E * (g * SWH/U^2)^{-0.55 \pm 0.23}. \quad (13b)$$

An important difference between formulas (10) and (13a) relating β with the wave-age needs to be pointed out. In (10) C_o/U is the true, measured wave-age while in (13a), ξ is a pseudo wave-age estimate from Hasselmann *et al.* [17] like expressions once the dimensionless significant height is known from altimeter measurements. ξ_m is defined as the pseudo wave-age world average whose value is not yet well defined [20], [21]. The coefficient E in (13b) clearly depends on ξ_m [with $\xi_m = 2.3$, as suggested by the authors, $E = 0.0097$; with $\xi_m = 1.1$, $E = 0.0049$ which appears in (11)]. The concept of pseudo-wave age was introduced by Fu and Glazman [19] to account for the presence of swell. In applying the concept,

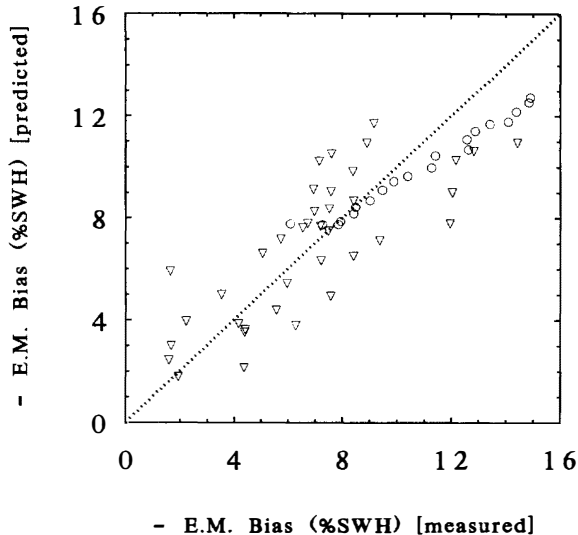


Fig. 16. Normalized EM bias predicted by: “ $\beta = -0.0049 * (g * SWH/U^2)^{-0.62}$ ” versus measured EM bias. (○) wind waves, (△) mixed waves.

one would expect significant reduction of the scatter noticed for mixed-waves runs.

In the IMST large wind wave facility, expressions similar to those of Hasselmann *et al.* [17] apply to the evolution of the dimensionless dominant frequency $n_o * U/g$ and the dimensionless mean energy $g^2 * SWH^2/U^4$ with respect to the dimensionless fetch $g * X/U^2$ [47]. When used to display the EM bias as a function of a pseudowave age, they do not yield any reduction of the scatter, which remains similar to what is shown on Fig. 15 for mixed-wave runs. This is not surprising as the pseudowave age is determined from expressions strictly valid for pure wind-wave fields in local equilibrium state. In this case there exists a one to one correspondence between the wave-age and the dimensionless wave-height, whereas with a swell the correspondence breaks down. Given a dimensionless significant wave-height, it appears not tenable to define an “equivalent” equilibrium state by simply introducing a pseudo wave-age. This leads us to conclude that in the presence of swell a simple quantity ξ or $g * SWH/U^2$ would be insufficient to predict EM bias.

The data scatter using formula (11) is shown on Fig. 16 and clearly the scatter is large. Recently Rodriguez *et al.* [8] pointed out *two mechanisms* underlying the EM bias: the modulation of small waves along the long waves and the long wave tilt modulation. So we proposed to explain the origin of the scatter by a *two-parameter model*, using dimensionless wave-height and wave-slope. Both pure wind waves and mixed seas can be represented by this model. A two parameter representation should involve information on both wave-height and wave-slope because EM bias is the mean *height* of the zero *slope* facets. So we introduce the significant slope ξ , and the two parameter representation of the normalized EM bias is in terms of *significant slope and nondimensional significant*

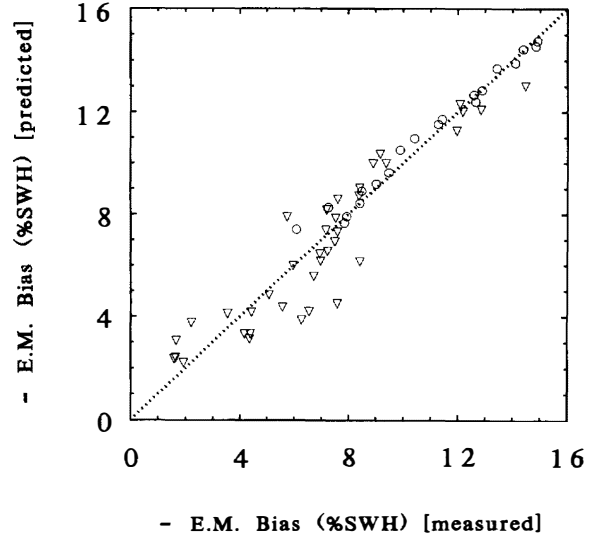


Fig. 17. Normalized EM Bias predicted by: “ $\beta = -0.167 * \xi^{+0.56} * (g * SWH/U^2)^{-0.34}$ ” versus measured EM bias. (●) wind waves, (△) mixed waves.

height, as

$$\beta = -0.167 * \xi^{+0.56 \pm 0.07} * (g * SWH/U^2)^{-0.34 \pm 0.05}$$

$$r^2 = 0.92 \quad (14)$$

This model provides close agreement with all of the laboratory data for both pure wind and combined conditions as shown in Fig. 17. This result helps us to understand EM bias on physical basis but its application awaits a viable technique for measuring ξ from altimetric data.

VI. DISCUSSION AND CONCLUSION

During this work we were primarily concerned with the physical mechanism involved in the interactions between microwave and water-surface waves. Of main interest was the dependence of the microwave backscattered signal on the sea state or on specific event occurring in the wave field. In that respect, it is known from previous investigations of Kwoh and Lake [48], Banner and Fooks [49], Lifermann *et al.* [24] that experiments in a wave tank offer unique advantage of allowing accurate control of the observational conditions. As a consequence, basic facts such as the sensitivity of the backscattered signal to the modulational instability or breaking of the surface waves were identified.

The illuminated spot size was small, so time series data were used in an analysis of pdf distributions to quantify the backscattered power as a function of wave phases. Generally the long-wave troughs were better reflectors than the long-wave crests. But this crest-to-trough asymmetry, which was measured in terms of EM bias, depended on local conditions. The goal of this paper was not to produce results for direct application to satellite altimetry, but rather to help to evaluate how robustly some empirical EM bias models characterize diverse data sets.

The analysis of open field observations and laboratory observations shows the inadequacy of EM bias parameterizations in terms of dimensional quantities. On the other hand, the data sets provide evidence that some recent parameterizations using nondimensional variables are quite robust. The laboratory data, however indicate that a new combination of nondimensional variables, which uses significant wave-height and significant wave-slope, is needed to effectively model diverse wave conditions.

Although some of the EM bias models we presented include field data, full application to field conditions needs further consideration of specific problems. Among others is the focusing effect due to range limitations. This may lead to an additional bias towards the wave troughs. Under the specific geometry of our observations, this bias would be small with respect to the first order bias associated with the wave-field nonlinearity. The high EM bias values measured in the tank were not due to an additional built-in bias: they were mainly due the nonlinear wave-field characterized by high skewness values of the wave height distributions. This is the physical law demonstrated by Jackson [9] and illustrated in Fig. 12.

While comparing laboratory and field situations, of more importance would be the reinforcement effect which occurs when there is a coherent combination of reflection elements distributed across all, or a portion, of the footprint. The associated spatial scale parameter may significantly differ from laboratory to field conditions. This laboratory data set can contribute to a better understanding of what is going on. Clearly, further progress will require both improved instrumentation and analytical studies. For example, significant slope seems to be unobtainable with present single-frequency altimeter design but perhaps future satellite-borne systems will use an enhanced design (building upon ROWS concepts [50]) or include complementary instruments such as an altimeter and a SAR. On the other hand, only a few investigations have been devoted to understanding the physical mechanisms. A numerical study by Poitevin *et al.* [51] shows that a modulated waveform produced by the instability of an initially uniform Stokes wave at moderate steepness yields absolute bias oscillating between one to four times the bias value for the Stokes wave. Ioualalen *et al.* [41] found that a two-dimensional wavefield with short crested waves yields an absolute bias higher than that of a one-dimensional wavefield for a same value of the significant slope. Rodriguez *et al.* [8] reported that both the modulation of small-scale waves and the modulation of large-scale surface tilt contribute roughly the same amount to the bias. Additional research is needed to quantify local variability of wave fields in order to develop more realistic statistical models for EM bias.

ACKNOWLEDGMENT

We are very grateful to C. Parsons who generously loaned the large focusing lens. We especially thank B. Zucchini for his diligent laboratory assistance. We acknowledge Dr. A. Lifermann for valuable discussions on

radar measurements. We acknowledge the helpful comments of anonymous reviewers who alerted us to the need for further investigation of the focusing effect.

REFERENCES

- [1] B. S. Yapple, A. Shapiro, D. L. Hammond, B. D. Au, and E. A. Uliana, "Nanosecond radar observations of the ocean surface from a stable platform," *IEEE Trans. Geosci. Electron.*, vol. GE-9, no. 3, pp. 170-174, 1971.
- [2] E. Rodriguez, "Altimetry for non Gaussian Oceans: height biases and estimation of parameters," *J. Geophys. Res.*, vol. 93, no. C11, pp. 14107-14120, 1988.
- [3] E. J. Walsh, C. J. Jackson, E. A. Uliana, and N. S. Swift, "Observation of electromagnetic bias in radar altimeter sea surface measurements," *J. Geophys. Res.*, vol. 94, no. C10, pp. 14575-14584, 1989.
- [4] J. J. Dудis, "Electromagnetic bias of airborne off-nadir laser backscatter from the Ocean," *J. Geophys. Res.*, vol. 91, no. C9, pp. 10750-10752, 1986.
- [5] R. Glazman and S. Pilorz, "Effects of sea maturity on satellite altimeter measurements," *J. Geophys. Res.*, vol. 95, no. C3, pp. 2857-2870, 1990.
- [6] G. S. Hayne and D. W. Hancock, "Corrections for the effects of significant wave height and attitude on Geosat radar altimeter measurements," *J. Geophys. Res.*, vol. 95, no. C3, pp. 2837-2842, 1990.
- [7] E. J. Walsh, F. C. Jackson, D. E. Hines, C. Piazza, L. G. Hevizi, D. J. Mc Laughlin, R. E. McIntosh, R. N. Swift, J. F. Scott, J. K. Yungel, and E. B. Frederick, "Frequency dependence of Electromagnetic Bias in radar altimeter sea surface range measurements," *J. Geophys. Res.*, vol. 96, no. C11, pp. 20571-20583, 1991.
- [8] E. Rodriguez, Y. Kim, and J. M. Martin, "The effect of small wave modulation on the electromagnetic Bias," *J. Geophys. Res.*, vol. 97, no. C2, pp. 2379-2389, 1992.
- [9] F. C. Jackson, "The reflexion of impulses from a non linear random sea," *J. Geophys. Res.*, vol. 84, no. C8, pp. 4939-4943, 1979.
- [10] E. Rodriguez and B. Chapman, "Extracting ocean surface information from altimeter returns: the deconvolution method," *J. Geophys. Res.*, vol. 94, no. C7, pp. 9761-9778, 1989.
- [11] E. Dobson, F. Monaldo, and J. Goldhirsh, "Validation of GEOSAT altimeter derived wind speeds and significant wave heights using buoy data," *J. Geophys. Res.*, vol. 92, no. C10, pp. 10719-10731, 1987.
- [12] W. K. Melville, R. H. Stewart, W. C. Keller, J. A. Kong, D. V. Arnold, A. J. Jessup, M. R. Loewen, and A. M. Slinn, "Measurements of Electromagnetic Bias in Radar Altimetry," *J. Geophys. Res.*, vol. 96, no. C3, pp. 4915-4924, 1991.
- [13] M. A. Srokosz, "On the joint distribution of surface elevation and slopes for a nonlinear random sea, with an application to radar altimetry," *J. Geophys. Res.*, vol. 91, no. C1, pp. 995-1006, 1986.
- [14] D. E. Barrick and B. J. Lipa, "Analysis and interpretation of altimeter sea echo," *Adv. Geophys.*, vol. 27, pp. 61-100, 1985.
- [15] G. S. E. Lagerloef, "Comment on 'On the joint distribution of surface elevation and slopes for a nonlinear random sea, with an application to radar altimetry' by M. A. Srokosz," *J. Geophys. Res.*, vol. 92, no. C3, pp. 2985-2987, 1987.
- [16] M. A. Srokosz, "Reply," *J. Geophys. Res.*, vol. 92, no. C3, pp. 2989-2990, 1987.
- [17] K. Hasselmann *et al.*, "Measurements of wind wave growth and swell decay during JONSWAP," *Herausgegeben vom Deutch Hydrograph Inst. Riehe A*, vol. 12, 95 pp., 1973.
- [18] R. E. Glazman and M. A. Srokosz, "Equilibrium wave spectrum and Sea State Bias in Satellite Altimetry," *J. Phys. Ocean.*, vol. 21, pp. 1609-1621, 1991.
- [19] L. Fu and R. Glazman, "The effect of wave age on the sea state bias in radar altimetry measurements," *J. Geophys. Res.*, vol. 96, no. C1, pp. 829-834, 1991.
- [20] W. J. Pierson, "Comment on 'Effects of sea maturity on satellite altimeter measurements' by R. Glazman and S. Pilorz," *J. Geophys. Res.*, vol. 96, no. C3, pp. 4973-4977, 1991.
- [21] R. Glazman, "Reply," *J. Geophys. Res.*, vol. 96, no. C3, pp. 4979-4983, 1991.
- [22] P. S. Callahan *et al.*, "WFF TOPEX Algorithm Specification—Electromagnetic (EM) Bias," TOPEX/POSEIDON Project, TOPEX Ground System, Science Algorithm Specification, JPL D-7075 Rev A, Change 1, Vers F1.1, pp. 163-169, 1991.
- [23] R. H. Stewart, "E. M. bias," communication at the Topex-Poseidon Science Working Team Meeting Workshop, Toulouse, Oct. 21-25, 1991.

- [24] A. Lifermann, B. Jähne and A. Ramamonjariisoa, "Une étude en soufflerie de la flexion hyperfréquences par les champs de houle et de vagues," *Oceanologica Acta*, No SP, Spacial Oceanography Symposium, Proceedings, pp. 15-22, 1987.
- [25] C. L. Parsons and L. S. Miller, "A laboratory study of the Electromagnetic Bias of rough surface scattering by water waves," *IEEE Trans. Geosci. Remote Sensing*, vol. 28, no. 6, pp. 1001-1011, 1990.
- [26] N. E. Huang, S. R. Long, and C. C. Tung, "The non-Gaussian joint probability density function of slope and elevation for a nonlinear gravity wave field," *J. Geophys. Res.*, vol. 89, no. C2, pp. 1961-1972, 1984.
- [27] M. Coantic and A. Favre, "Activities in, and preliminary results of, air sea interaction research at I.M.S.T.," *Adv. Geophys.*, vol. 91, pp. 391-405, 1974.
- [28] A. Ramamonjariisoa "Contribution à l'étude de la structure statistique et des mécanismes de génération des vagues de vent." Thèse de Doctorat d'Etat, Université de Provence, IMST, Marseille, 1974, pp. 300.
- [29] O. M. Phillips, *The Dynamic of the Upper Ocean*, 2nd. Ed. New York: Cambridge University Press, New York, 1977.
- [30] L. F. Bliven and G. Norcross, "Effect of rainfall on scatterometer derived wind-speeds," in *Proc. IGARSS'88*, Edinburgh, Scotland, Sept. 12-16, 1988, ESA SP-284 (Paris: European Space Agency), vol. 1, 1988, pp. 565-566.
- [31] J. P. Giovanangeli, L. F. Bliven, and O. Le Calvé, "A wind-wave tank study of the azimuthal response of a Ka-band scatterometer," *IEEE Trans. Geosci. Remote Sensing.*, vol. 29, no. 1, pp. 143-148, 1991.
- [32] L. F. Bliven and J. P. Giovanangeli, "An experiment Study of Microwave Scattering From Rain and Wind-Roughened Seas," *Int. J. Remote Sensing*, vol. 14, no. 5, pp. 855-869, 1993.
- [33] L. S. Miller, "A 35 GHz instrumentation radar for very high resolution measurements," Task IV Final Report, NASA contract NAS6-3120, 24 pp., July 1983.
- [34] D. J. Kirchner, "Removal of interference inherent in the lens radar system," M.S. thesis, Virginia Polytechnic Inst. State Univ., June 6, 130 pp., 1988.
- [35] D. J. Kirchner, G. Brown, and B. Davis, "Research on multibeam Altimetry and Electromagnetic Bias," Final Report, NASA contract 230-11-35451, GSFC, Wallops Fl. Fac. 76 pp., 1988.
- [36] G. S. Brown, "The average impulse response of a rough surface and its applications," *IEEE Trans. Antennas and Propagat.*, vol. AP-25, no. 1, pp. 67-74, 1977.
- [37] P. Bonmarin, "Geometric properties of deep water breaking waves," *J. Fluid Mech.*, vol. 209, pp. 405-433, 1989.
- [38] C. C. Tung, N. E. Huang, Y. Yuan, and R. Long., "Probability density function of breaking-limited surface elevation," *J. Geophys. Res.*, vol. 94, no. C1, pp. 967-972, 1989.
- [39] D. J. Carter, Challenor P. G. and M. A. Srokosz, "An assessment of Geosat wave height and windspeed measurements," *J. Geophys. Res.*, vol. 97, no. C7, pp. 11383-11392, 1992.
- [40] A. Guillaume and N. Mognard, "A new method for the validation of altimeter-derived sea-state parameters with results from wind and wave models," *J. Geophys. Res.*, vol. 97, no. C6, pp. 9705-9717, 1992.
- [41] M. Ioualalen, J. Poitevin, and C. Kharif, "Effect of three dimensional wavefields on the altimeter response," in *Proc. IGARSS'91 Symposium*, Helsinki, vol. 2, 1991, pp. 483-485.
- [42] E. J. Walsh, "Interim coefficients for TOPEX E.M. Bias algorithm," personal note distributed to the Topex-Poseidon Science Working Team, 1991.
- [43] D. L. Witter and B. Chelton, "An apparent wave-height dependence in the sea-state bias in GEOSAT altimeter range measurements," *J. Geophys. Res.*, vol. 96, no. C5, pp. 8861-8867, 1991.
- [44] R. Ray and C. Koblinsky, "On the sea state bias of the Geosat altimeter," *J. Atmos. Ocean. Tech.*, vol. 8, pp. 397-408, 1991.
- [45] L. W. Choy, D. L. Hammond, and E. A. Uliana, "Electromagnetic bias of 10-GHz radar altimeter measurements of MSL" *Mar. Geod.*, vol. 8, pp. 297-312, 1984.
- [46] C. Cox and W. Munk, "Statistics of the sea surface derived from sun glitter," *S. Found J. Mar. Res.*, vol. 13, pp. 198-227, 1954.
- [47] A. Ramamonjariisoa, "Sur l'évolution des spectres d'énergie des vagues de vent à fetch court," *Mem Soc. Roy. Liege*, vol. 6, no. 7, pp. 47-66, 1973.
- [48] D. S. Kwoh and B. M. Lake, "The nature of microwave backscattering from water waves," Report TRW Space and Technology Group, Cal. 90278, 1984.
- [49] M. L. Banner and E. H. Fooks, "On the microwave reflectivity of small scale breaking waves," *Proc. Roy. Soc. London*, Ser. A, 399, pp. 93-109, 1985.
- [50] F. C. Jackson, W. T. Walton, and P. L. Baker, "Aircraft and satellite measurement of ocean wave directional spectra using scanning-beam microwave radars," *J. Geophys. Res.*, vol. 90, no. C1, pp. 987-1004, 1985.
- [51] J. Poitevin, A. Ramamonjariisoa, and C. Kharif, "Altimeter response to nonlinear surface wave fields," in *Proc. IGARSS'90*, Washington, vol. 1, 1990, pp. 699-702.
- [52] M. S. Longuet-Higgins, "The effect of non linearities on statistical distributions in the theory of sea waves," *J. Fluid Mech.*, vol. 17, pp. 459-480, 1963.